American Mineralogist, Volume 91, pages 247–251, 2006

Pressure-induced hydration in zeolite tetranatrolite

YONGJAE LEE,[1,*] JOSEPH A. HRILJAC,[2] JOHN B. PARISE,[3] AND THOMAS VOGT[1]

[1]Department of Earth System Sciences, Yonsei University, Seoul 120749, Korea and
Physics Department, Brookhaven National Laboratory, Upton, New York 11973, U.S.A.
[2]School of Chemistry, University of Birmingham, Birmingham, B15 2TT, U.K.
[3]Geosciences Department, State University of New York, Stony Brook, New York 11794, U.S.A.

ABSTRACT

The tetranatrolite-paranatrolite transformation has remained a key problem in understanding the paragenesis of zeolites in the natrolite family. It is accepted that when paranatrolite, approximate formula $Na_{16-x}Ca_xAl_{16+x}Si_{24-x}O_{80}\cdot 24H_2O$, is removed from an aqueous environment and exposed to the atmosphere, it loses water and transforms to tetranatrolite, $Na_{16-x}Ca_xAl_{16+x}Si_{24-x}O_{80}\cdot nH_2O$ ($n \le 24$). Here we show that this transformation is not only reversible, but that tetranatrolite exhibits two sequential pressure-induced hydrations leading first to paranatrolite and then to a superhydrated tetranatrolite above 0.2 and 3.0 GPa, respectively. We have previously reported similar behavior for the corresponding system with an ordered Si/Al distribution, i.e., natrolite itself, however the ordered version of paranatrolite exists over a much smaller pressure range. The pressure-induced transformations of natrolite and tetranatrolite thus further supports the supposition that paranatrolite is a distinct mineral species, with a pressure-stability field dependent upon composition.

Keywords: Crystal structure, high pressure, phase transition, tetranatrolite, paranatrolite, synchrotron X-ray powder diffraction, pressure-induced hydration

INTRODUCTION

The structures and compositions of zeolite minerals are of prime importance in understanding their origin and effectiveness as host materials in numerous environmental and industrial applications (Breck 1984). The natrolite mineral group occurs in geological environments ranging from deep marine to the vugs and cavities in basalts and are an important phase for thermodynamic modeling of the stable zeolite assemblages in the environments in which they occur. Unfortunately this modeling is complicated in most zeolitic systems. It is particularly complex in the case of the natrolite group because of controversy over their compositions, stability, and existence (or not) of distinct forms with different states of hydration, cation stoichiometry, and Si/Al ordering. The simplest system is the parent natrolite, $Na_{16}Al_{16}Si_{24}O_{80}\cdot 16H_2O$, whose structure was first reported by Pauling and Taylor in the early 1930s (Pauling 1930; Taylor et al. 1933). The framework of fibrous zeolites is composed of chains of tetrahedra interconnected to form elliptical channels along the **c** axis (Baur et al. 1990; Meier 1960; Alberti et al. 1995). In natrolite, silicon and aluminum atoms in a 3:2 ratio are ordered and occupy different framework tetrahedral (T) sites. The sodium cations and water molecules also adopt ordered arrangements along the channel. Depending on their geological settings, chemical substitutions occur either in the natrolite framework or at the charge-balancing cation sites, giving rise to a variety of analog mineral species such as scolecite, $Ca_8Al_{16}Si_{24}O_{80}\cdot 24H_2O$ (Kvick et al. 1985), mesolite, $Na_{5.3}Ca_{5.3}Al_{16}Si_{24}O_{80}\cdot 21.3H_2O$ (Artioli et al. 1986), gonnardite (Artioli and Galli 1999), and tetranatrolite (Evans et al. 2000). In scolecite and mesolite, the framework maintains an ordered Si/Al arrangement in a 3:2 ratio. However, different degrees of Ca-exchange for Na leads to a monoclinic distortion or a tripling of the *b* axis of the parent orthorhombic natrolite unit cell, respectively. The compositions and structural relationship between gonnardite and tetranatrolite remains controversial (Artioli and Galli 1999; Evans et al. 2000; Ross et al. 1992) but they have been reported to have the representative formulae $Na_{16-x}Ca_xAl_{16+x}Si_{24-x}O_{80}\cdot nH_2O$ ($0.2 \le x \le 3.9$, $16 \le n \le 25.2$) with disordered Si/Al distributions at the framework T-sites and partial Ca-water substitution at the nonframework sites. Paranatrolite is another natrolite analog with a high water content, $Na_{16-x}Ca_xAl_{16+x}Si_{24-x}O_{80}\cdot nH_2O$ or ideally, $Na_{16}Al_{16}Si_{24}O_{80}\cdot nH_2O$, n ~ 24 (Chao 1980; Ross et al. 1992). Paranatrolite is reported to transform to tetranatrolite upon exposure to the atmosphere after removal from its aqueous environment (Chao 1980). It has been also suggested that tetranatrolite is a dehydration product of paranatrolite that crystallizes within a particular temperature and humidity range (Evans et al. 2000). Recently, Seryotkin et al. (Seryotkin et al. 2004) reported the structure of paranatrolite using a single crystal preserved in a water-filled capillary at ambient conditions. The dehydration of paranatrolite to tetranatrolite has been believed to be *irreversible*, and no evidence yet exists of the tetranatrolite to paranatrolite transformation.

We have recently shown that the volume expansion of natrolite with an ordered Si/Al distribution at pressures above 1.0 GPa occurs in two steps via the selective sorption of water molecules from the hydrostatic pressure transmitting fluid (Lee et al. 2001, 2002). This pressure-induced hydration (PIH) first increases the crystal water content from 16 to 24 (per 80 framework O atoms) leading to a form of paranatrolite with an ordered Si/Al

* E-mail: yongjaelee@yonsei.ac.kr

framework at 1.0 GPa and then to a fully superhydrated phase with 32 water molecules above 1.2 GPa. The latter transition is reversible whereas the ordered paranatrolite phase exhibits a large hysterisis upon pressure release and coexists with the original natrolite as long as it is kept in a water-filled sample chamber (Lee et al. 2005a). Our results thus demonstrated that pressure-induced hydration is a mechanism to vary zeolitic water contents in the natrolite family and hence, provided new insights into the origin of the paranatrolite phase. To explore the possible tetranatrolite to paranatrolite transformation and understand the role of the framework Si/Al ratio and subsequent nonframework cation-water substitution on pressure-induced hydration, another set of experiments were performed using tetranatrolite from Mt. St. Hilaire. This has a disordered Si/Al distribution and is thought to be the *irreversible* phase transformation product from natural paranatrolite (Chao 1980; Evans et al. 2000; Lee et al. 2005a). In this paper we show for the first time that the paranatrolite to tetranatrolite transformation is *reversible* through pressure-induced hydration. We therefore find that paranatrolite is indeed a distinct mineral species, which can be formed at high pressure either from natrolite or tetranatrolite with a stability field that varies with composition.

Experimental methods

Variable-pressure powder diffraction measurements were performed using a diamond-anvil cell (DAC) at beamline X7A at the National Synchrotron Light Source (NSLS). A powdered sample of tetranatrolite (from Mt. Saint-Hilaire, NMNH-R18930; white polycrystalline overgrowths on the surfaces of natrolite single crystals, EPMA: $Na_{11.7}Ca_{3.8}Al_{18.5}Si_{21.5}O_{80}{\cdot}nH_2O$) was loaded into a 200 µm diameter sample chamber in a pre-indented stainless steel gasket, along with a few small ruby chips as a pressure gauge (Bell and Mao 1979). A mixture of 16:3:1 by volume of methanol:ethanol:water was used as a pressure medium (hydrostatic up to ~10 GPa). The pressure at the sample was measured by detecting the shift in the R1 emission line of the included ruby chips. The sample was equilibrated for about 30 min at each pressure, and diffraction data were collected using a horizontally focused (~200 µm) monochromatic X-ray beam [λ = 0.6834(1) Å] with an asymmetrically cut bent Si (111) monochromator (Lemonnier et al. 1978) and a gas-proportional position-sensitive detector (Smith 1991). A monoclinic phase, with a similar volume expansion yet less pronounced peak splitting than the one observed in the natrolite experiment (Lee et al. 2005a), started to appear near 0.2(1) GPa as a secondary phase next to the original tetragonal phase. Subsequently a pure monoclinic phase formed upon further pressure increase and persisted up to 2.5(1) GPa. Above 4.2(1) GPa, a single tetragonal phase was observed, followed by gradual peak shifts to higher 2θ values up to a final pressure of 6.9(1) GPa. Upon full pressure release, a tetragonal phase was observed with a unit cell volume slightly larger (by ca. 0.4%) than the one measured before the pressure cycle. No evidence of nonhydrostatic conditions or pressure anisotropy was detected during our experiments.

Results and discussion

The changes in the unit-cell parameters and volume of tetranatrolite as a function of hydrostatic pressures up to 6.9(1) GPa are shown in Figure 1. For comparison, data from previous natrolite experiments are also plotted. In contrast to natrolite, tetranatrolite exhibits a volume expansion and monoclinic distortion at pressures as low as 0.2 GPa and up to 2.5(1) GPa (Fig. 1). The degree of volume expansion in tetranatrolite is only ca. 2.0%, compared to ~7.0% expansion in natrolite at 1.0 GPa, because the ambient pressure phase already contains more water molecules in a larger unit cell: 22 H_2O per 80 framework O atoms (O_f), based on the ambient pressure structure refinement, compared to 16 H_2O per 80 O_f in ambient natrolite. This intermediate monoclinic phase then transforms to a new tetragonal phase above 3 GPa with ca. 2.4% volume reduction. Further increase of the pressure up to 6.9(1) GPa reveals no further volume anomally, and the original tetranatrolite phase is recovered upon full pressure release.

The structures of the high-pressure phases were examined using Rietveld methods (Rietveld 1969; Young 1995) and the GSAS suite of programs (Larson and VonDreele 1986; Toby

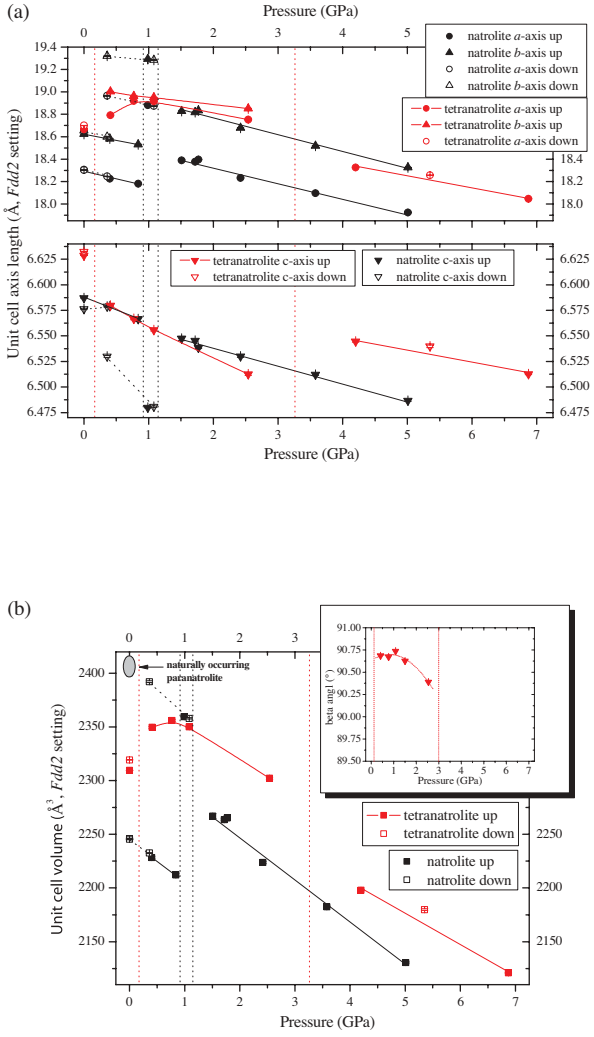

Figure 1. Pressure-dependent evolution of (**a**) unit-cell edge lengths and (**b**) unit-cell volume, normalized to the orthorhombic setting with 80 framework O atoms, in natrolite ($Na_{16}Al_{16}Si_{24}O_{80}{\cdot}nH_2O$, n = 16 at 1 bar, black symbols) and tetranatrolite ($Na_{11.7}Ca_{3.8}Al_{18.5}Si_{21.5}O_{80}{\cdot}nH_2O$; n = 22 at 1 bar, red symbols) under hydrostatic pressures mediated by an alcohol and water mixture. The inset in (**b**) shows the pressure evolution of the monoclinic beta angle. Filled symbols represent data taken on pressure increase and unfilled symbols during pressure release. Data from Lee et al. (2002) were used to represent the natrolite experiment. Dotted vertical lines show the expected paranatrolite region in tetranatrolite (red) and natrolite (black). For comparison, a grey ellipse is shown to represent the region of the reported volumes of naturally occurring paranatrolite at ambient pressure: a = 19.07(1) Å, b = 19.13(1) Å, c = 6.580(3) Å, V = 2400 Å^3 by Chao (1980); a = 19.02(1) Å, b = 19.20(1) Å, c = 6.606(4) Å, β = 91.56(4)°, V = 2412 Å^3 by Paukov et al. (2002).

TABLE 1. Final refined atomic coordinates for tetranatrolite (at ambient conditions) and superhydrated tetranatrolite (above 3 GPa)†

Pressure		Ambient*	4.2(1) GPa	6.9(1) GPa	5.4(1) GPa on release
Space group		$I\bar{4}2d$	$I\bar{4}2d$	$I\bar{4}2d$	$I\bar{4}2d$
${}_wR_p$ (%), R_p (%)		2.85, 2.14	3.95, 2.95	3.67, 2.78	4.17, 3.06
χ^2, $R(F^2)$ (%)		5.5, 7.3	3.9, 16.0	4.5, 17.6	6.3, 19.1
water molecules/80 O_f		21.9(1)	32	32	32
cell length (Å)	*a*	13.1988(1)	12.959(1)	12.761(1)	12.910(2)
	c	6.6288(1)	6.5446(7)	6.5127(6)	6.540(1)
T1	*x*	0	0	0	0
4a	*y*	0	0	0	0
	z	0	0	0	0
	U_{iso}	0.0080(2)	0.028(1)	0.026(1)	0.022(1)
T2	*x*	0.0550(1)	0.0538(3)	0.0552(2)	0.0575(4)
16e	*y*	0.1326(1)	0.1314(3)	0.1328(2)	0.1351(4)
	z	0.6210(1)	0.6198(3)	0.6212(2)	0.6235(4)
O1	*x*	0.3918(3)	0.399(1)	0.379(1)	0.379(2)
8d	*y*	0.25	0.25	0.25	0.25
	z	0.125	0.125	0.125	0.125
	U_{iso}	0.0120(5)	0.028(1)	0.026(1)	0.022(1)
O2	*x*	0.1339(2)	0.140(8)	0.144(1)	0.138(1)
16e	*y*	0.0607(2)	0.055(1)	0.050(1)	0.045(1)
	z	0.4780(4)	0.521(2)	0.542(1)	0.531(2)
O3	*x*	0.0526(2)	0.036(1)	0.017(1)	0.020(1)
16e	*y*	0.0951(2)	0.115(1)	0.111(1)	0.110(1)
	z	0.8662(3)	0.885(1)	0.873(1)	0.873(1)
Na	*x*	0.6923(2)	0.695(1)	0.694(1)	0.691(1)
8d	*y*	0.25	0.25	0.25	0.25
	z	0.125	0.125	0.125	0.125
	Occu.	0.731	0.731	0.731	0.731
	U_{iso}	0.0268(8)	0.028(1)	0.026(1)	0.022(1)
Ca	*x*	0.6923(2)	0.695(1)	0.694(1)	0.691(1)
8d	*y*	0.25	0.25	0.25	0.25
	z	0.125	0.125	0.125	0.125
	Occu.	0.237	0.237	0.237	0.237
OW4	*x*	0.1277(4)	0.130(1)	0.125(1)	0.131(2)
8d	*y*	0.25	0.25	0.25	0.25
	z	0.125	0.125	0.125	0.125
	Occ.	1	1	1	
	U_{iso}	0.038(1)	0.028(1)	0.026(1)	0.022(1)
OW5	*x*	0.875(1)	0.897(1)	0.889(1)	0.898(2)
8d	*y*	0.25	0.25	0.25	0.25
	z	0.125	0.125	0.125	0.125
	Occ.	0.370(6)	1	1	1

P (GPa)	ambient	0.4	0.8	1.1	1.5	2.5	4.2	6.9	$5.4^{(on\ release)}$	$ambient^{(on\ release)}$
V (Å^3)	2309.6(1)	2361.1(5)	2368.5(4)	2348.9(5)	2335.6(5)	2318.5(5)	2198.0(5)	2121.0(4)	2179.8(8)	2319.3(3)

* Data measured using dry powder sample contained inside a capillary holder (Lee et al. 2005b).

† E.s.d.s are in parentheses. Na and Ca occupancies were fixed according to the elemental analysis results as well as the T-sites to contain 53.7% Si and 46.3% Al. Site occupancies for the OW4 and OW5 sites were fixed to unity for high-pressure models; when refined they become slightly larger than unity. Restraints were used to set the isotropic displacement factors, U_{iso} (Å^2), equal for the same atomic species (response to ambient model) or for the all atoms (for high pressure models). Soft constraints were used for the framework interatomic distances for the high pressure models [T-O = 1.677(1) Å and O-O = 2.739(5) Å].

2001) (Tables 1–2). The intermediate phase formed from tetranatrolite between 0.4(1) and 2.5(1) GPa could be indexed using a monoclinic *Cc* space group, as is the case for ordered paranatrolite formed from natrolite at 1 GPa (Lee et al. 2005a) and paranatrolite itself at ambient conditions (Seryotkin et al. 2004). Although Rietveld analysis proved the nature of the material is indeed paranatolite, the complexity of the structural model and modest quality of the powder pattern made extracting details problematic. However, based on the similarity of unit cell volume near 1 GPa (Fig. 1b), we can expect that the intermediate phase would exhibit an increased water content of ~24 H_2O per 80 O_f. This would then lead to a marginal density reduction compared to ordered paranatrolite (Fig. 2).

The pressure-induced hydration of tetranatrolite points to a new assembly of the confined water molecules and charge-balancing cations inside the channels, which evolves with increasing pressure as the water content increases and the zeolitic scaffolding swells. At ambient conditions, the sodium and calcium cations are disordered over the same site; this mixed cation occupancy model has been assumed throughout the refinements of the high-pressure structural models (Table 1). At ambient conditions, the water sites along both corners of the channel ellipses (OW5) are partially filled (Fig. 3). We speculate that the intermediate monoclinic phase with ~24 H_2O per 80 O_f is characterized by the disordering and increased occupancy of the partially filled water sites, similar to the proposed structural model for naturally occurring paranatrolite at ambient conditions (Seryotkin et al. 2004). More detailed structural analysis of the intermediate phase will be addressed in future studies. Above 3 GPa, full PIH with 32 H_2O per 80 O_f occurs, and the intermediate pressure monoclinic phase transforms to a high-pressure tetragonal phase (Table 1). At this point a fully connected, three dimensional water network is formed, which persists up to the final pressure of 6.9(1) GPa (Fig. 3 and Table 2).

In summary, we have demonstrated that natrolite and tetranatrolite, with ordered and disordered Si/Al distributions, respec-

TABLE 2. Selected interatomic distances (Å) and angles (°) for tetranatrolite (at ambient conditions) and superhydrated tetranatrolite (above 3 GPa)*

	Ambient	4.2(1) GPa	6.9(1) GPa	5.4(1) GPa on release
T1-O3	1.686(3) × 4	1.732(7) × 4	1.656(4) × 4	1.665(6) × 4
T2-O1	1.702(2)	1.655(7)	1.718(6)	1.697(8)
T2-O2	1.698(3)	1.625(12)	1.632(7)	1.669(10)
T2-O2	1.662(3)	1.687(11)	1.720(8)	1.666(10)
T2-O3	1.699(2)	1.766(7)	1.733(5)	1.731(6)
Av. T-O†	1.690(1)	1.683(5)	1.701(3)	1.691(4)
T2-O1-T2	131.2(2)	136.5(11)	121.1(8)	121.9(11)
T2-O2-T2	136.6(2)	133.1(9)	129.9(7)	139.5(12)
T1-O3-T2	136.7(2)	124.4(5)	130.2(4)	132.4(5)
Na-O1	2.613(3) × 2	2.63(1) × 2	2.42(1) × 2	2.45(1) × 2
Na-O2	2.415(3) × 2	2.50(1) × 2	2.52(1) × 2	2.58(1) × 2
Na-O3				
Na-OW4	2.436(3) × 2	2.37(1) × 2	2.40(1) × 2	2.37(1) × 2
Na-OW5	2.41(1)	2.61(2)	2.50(2)	2.67(2)
OW4-O3	2.848(3) × 2	2.65(1) × 2	2.78(1) × 2	2.83(1) × 2
OW5-O1	2.995(6) × 2	3.17(1) × 2	2.92(1) × 2	3.01(1) × 2
OW5-O2	3.161(4) × 2	2.80(1) × 2	2.67(1) × 2	2.78(1) × 2
OW5-O3	2.637(3) × 2	2.78(1) × 2	2.91(1) × 2	2.92(1) × 2
		2.96(1) × 2	2.98(1) × 2	2.97(1) × 2
OW4-OW5	2.84(1) × 2	2.96(1) × 2	2.89(1) × 2	2.95(2) × 2
		3.02(2)	3.00(2)	3.01(3)

* E.s.d. values are in parentheses.
† Standard deviations are computed using $\sigma = \frac{1}{n}\left(\sum_{i=1}^{n}\sigma_i^2\right)^{1/2}$.

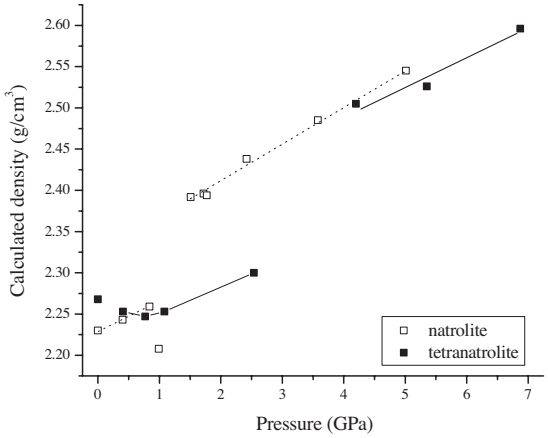

FIGURE 2. Pressure dependency of the calculated density in natrolite and tetranatrolite. Data from Lee et al. (2002) are used for the natrolite behavior (open symbols).

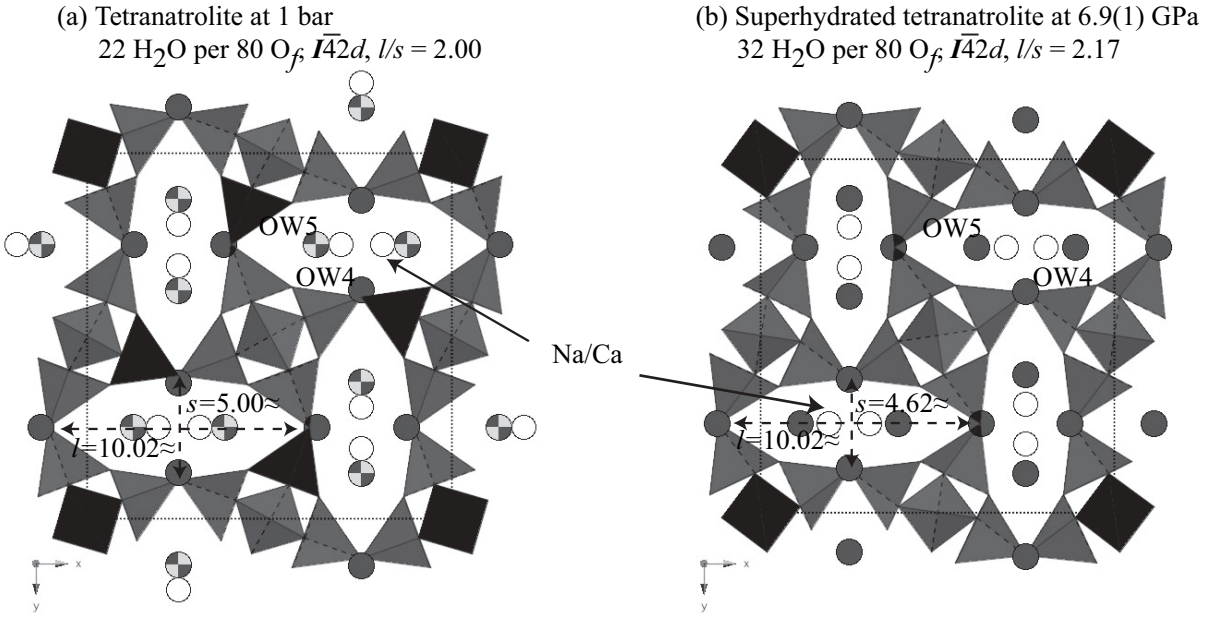

FIGURE 3. The evolution of the crystal structure of tetranatrolite ($Na_{11.7}Ca_{3.8}Al_{18.5}Si_{21.5}O_{80}{\cdot}nH_2O$; n = 22 at 1 bar) with pressure viewed parallel to the channel axis. (**a**) Tetranatrolite before PIH at 1bar, n = 22 per 80 framework O atoms, (**b**) superhydrated tetranatrolite at 6.9(1) GPa, n = 32. Tetrahedra are shown in one color to illustrate the disordering of Si/Al over the framework tetrahedral sites. Open circles represent mixed Na/Ca sites, and O atoms from water molecules are shown as two tone and filled cicles to illustrate partial and full occupancies, respectively. The ellipticity of the channel opening is illustrated by dotted arrows. Dotted lines define unit cells.

tively, transform *reversibly* to similar intermediate monoclinic phases upon partial pressure-induced hydration. These intermediate phases are identified as ordered and disordered forms of paranatrolite, respectively. The stability field of paranatrolite is apparently dependent upon the Si/Al-ordering and/or the different nonframework cation and water contents or distribution within the channels. The higher Si/Al ratio in tetranatrolite may be realized by substituting one Ca for one Na atom every time an extra Al atom goes into the framework. Coupled to this, more water must then go into the system to keep Ca 7-coordinated. This would then lead to an empirical formula for tetranatrolite (with the Ca-content adjustable by y) of $Na_{(16-x-2y)}Ca_{(x+y)}Al_{(16+x)}Si_{(24-x)}O_{(80)}$

$\cdot(16 + x + 2y)H_2O$. Based on this formula, our sample would have an ideal composition of $Na_{11.5}Ca_{3.5}Al_{18.5}Si_{21.5}O_{80}\cdot 19.5H_2O$, which is not far from our refined composition. It seems reasonable that the lower onset of pressure-induced hydration in tetranatrolite is due to its higher initial water content, a larger starting volume, and a more disrupted hydrogen bonding network due to the partial Ca-substitution. The reason for the wider pressure range is unclear, but we speculate that it indicates that in tetranatrolite, sevenfold coordination of the cation is partially realized in the paranatrolite stage due to partial Ca-substitution, and further hydration to 32 H_2O per 80 O_f would thus generate non-coordinating water molecules that are energetically less favorable. As shown by our natrolite experiments, paranatrolite may be recovered as a metastable phase upon pressure release as long as it is contained in an aqueous environment. Given the anomalous increase in the channel opening and changes in the cation coordination environment, one may expect an increased water mobility and ion exchange capacity in the paranatrolite phase.

ACKNOWLEDGMENTS

This work was supported by an LDRD from BNL ("Pressure in Nanopores"). The authors thank J. Post (Smithsonian Institution, USA) for providing mineral specimens of tetranatrolite. J. Hriljac acknowledges support from the Royal Society and J. Parise from NSF-DMR-0095633 and NSF-EAR-0125094. Y. Lee also thanks the Mineralogical Society of America for providing a Crystallographic Research Grant. Research carried out in part at the NSLS at BNL is supported by the U.S. DOE (DE-AC02-98CH10886 for beamline X7A). We gratefully acknowledge the Geophysical Laboratory of the Carnegie Institute for access to their ruby laser system at beamline X17C.

REFERENCES CITED

Alberti, A., Cruciani, G., and Dauru, I. (1995) Order-disorder in natrolite-group minerals. European Journal of Mineralogy, 7, 501–508.

Artioli, G. and Galli, E. (1999) Gonnardite: Re-examination of holotype material and discredition of tetranatrolite. American Mineralogist, 84, 1445–1450.

Artioli, G., Smith, J.V., and Pluth, J.J. (1986) X-ray structure refinement of mesolite. Acta Crystallographica, C42, 937–942.

Baur, W.H., Kassner, D., Kim, C.-H., and Sieber, N.H. (1990) Flexibility and distortion of the framework of natrolite: crystal structures of ion-exchanged natrolites. European Journal of Mineralogy, 2, 761–769.

Bell, P.M. and Mao, H.K. (1979) Absolute pressure measurements and their comparison with the ruby fluorescence (R1) pressure scale to 1.5 Mbar. Carnegie Institution of Washington Year Book, 78, 665–669.

Breck, D.W. (1984) Zeolite Molecular Sieves. Krieger, Malabar, Florida.

Chao, G.Y. (1980) Paranatrolite, a new zeolite from mont St-Hilaire, Quebec. Canadian Mineralogist, 18, 85–88.

Evans, H.T., Konnert, J.A., and Ross, M. (2000) The crystal structure of tetranatrolite from Mont Saint-Hilaire, Quebec, and its chemical and structural relationship to paranatrolite and gonnardite. American Mineralogist, 85, 1808–1815.

Kvick, A., Stahl, K., and Smith, J.V. (1985) A neutron diffraction study of the bonding of zeolitic water in scolecite at 20K. Zeitschrift für Kristallographie, 171, 141–154.

Larson, A.C. and VonDreele, R.B. (1986) GSAS; General Structure Analysis System. Los Alamos National Laboratory, New Mexico.

Lee, Y., Hriljac, J.A., Vogt, T., Parise, J.B., and Artioli, G. (2001) First structural investigation of a super-hydrated zeolite. Journal of the American Chemical Society, 123, 12732–12733.

Lee, Y., Vogt, T., Hriljac, J.A., Parise, J.B., and Artioli, G. (2002) Pressure-induced volume expansion of zeolites in the natrolite family. Journal of the American Chemical Society 124, 5466–5475.

Lee, Y., Hriljac, J.H., Parise, J.B., and Vogt, T. (2005a) Pressure-induced stabilization of ordered paranatrolite: A new insight into the paranatrolite controversy. American Mineralogist, 90, 252–257.

Lee, Y., Hriljac, J.A., and Vogt, T. (2005b) Variable-temperature structural studies of tetranatrolite from Mt. St. Hilaire; Synchrotron X-ray powder diffraction and Rietveld analysis. American Mineralogist, 90, 247–251.

Lemonnier, M., Fourme, R., Rosseaux, F., and Kahn, R. (1978) X-ray curved-crystal monochromator system at the storage ring DCI. Nuclear Instruments and Methods, 152, 173–177.

Meier, W.M. (1960) The crystal structure of natrolite. Zeitschrift für Kristallographie, 113, 430.

Paukov, I.E., Moroz, N.K., Kovalevskaya, Y.A., and Belitsky, I.A. (2002) Low-temperature thermodynamic properties of disordered zeolites of the natrolite group. Physics and Chemistry of Minerals, 29, 300–306.

Pauling, L. (1930) The structure of some sodium and calcium aluminosilicates. Proceedings of the National Academy of Sciences, 16, 453–459.

Rietveld, H.M. (1969) A profile refinement method for nuclear and magnetic structures. Journal of Applied Crystallography, 2, 65–71.

Ross, M., Flohr, M.J.K., and Ross, D.R. (1992) Crystalline solution series and order-disorder within the natrolite mineral group. American Mineralogist, 77, 685–703.

Seryotkin, Y.V., Bakakin, V.V., and Belitsky, I.A. (2004) The crystal structure of paranatrolite. European Journal of Mineralogy, 16, 545–550.

Smith, G.C. (1991) X-ray imaging with gas proportional detectors. Synchrotron Radiation News, 4, 24–30.

Taylor, W.H., Meek, C.A., and Jackson, W.W. (1933) The structures of the fibrous zeolites. Zeitschrift für Kristallographie, 84, 373.

Toby, B.H. (2001) EXPGUI, a graphical user interface for GSAS. Journal of Applied Crystallography, 34, 210–213.

Young, R.A. (1995) The Rietveld Method, 298 p. International Union of Crystallography, Oxford University Press, New York.

MANUSCRIPT RECEIVED NOVEMBER 8, 2004
MANUSCRIPT ACCEPTED JUNE 17, 2005
MANUSCRIPT HANDLED BY ALESSANDRO GUALTIERI